Fluorescence Studies of Pyrene Maleimide-Labeled Translin: Excimer Fluorescence Indicates Subunits Associate in a Tail-to-Tail Configuration to Form Octamer

Myun K. Han,*,# Paul Lin,‡ David Paek,# John J. Harvey,‡ Elena Fuior,# and Jay R. Knutson‡

Department of Microbiology and Immunology, Georgetown University Medical Center, Washington, DC 20007 and Laboratory of Biophysical Chemistry, National Heart, Lung and Blood Institute, National Institutes of Health, Bethesda, Maryland 20892

Received October 30, 2001

ABSTRACT: Translin is an octameric single-stranded DNA binding protein consisting of 228 amino acid residues per monomer. This protein contains two cysteine residues per monomer. Studies of reactions with DTNB show that both cysteines are reactive and exhibit biphasic reaction kinetics. Further studies with two site-directed mutants, C58S and C225S, confirm that Cys-58 reacts slowly while Cys-225 reacts quickly. Pyrene excimer emission was observed for pyrene maleimide-labeled C58S mutant. This was not observed, however, with the pyrene maleimide-labeled C225S mutant. DAS (decay associated spectra) revealed that all excited pyrene labels on C225 residues can form excimers with pyrenes of adjacent subunits within a few nanoseconds. Time-resolved emission anisotropy detects a rotational correlation time appropriate for octameric but not dimeric species. These results indicate proximity for the Cys-225 residues on adjacent monomers and that the subunits must interact in a tail-to-tail orientation. Moreover, disulfide bonds are not required for the formation of an octamer.

Chromosomal translocation is observed in many lymphoid malignancies (*1*). Translin, also referred to as testis−brain RNA binding protein (TB-RBP), is a recently identified, highly conserved nucleic acid-binding protein that recognizes many chromosomal breakage points and may be involved in chromosomal translocation (*2*−*4*). Although translin is primarily located in the cytoplasm, it is also found in the nucleus of lymphoid cells with rearranged immunoglobulin and T cell receptor loci (*3*). When DNA within cells is damaged with chemical agents such as mitomycin C, translin is transported from the cytosol into the nucleus, suggesting that translin has a role in both DNA recombination and repair (*5*). Moreover, translin may be important in recognizing chromosomal breakpoints in solid tumors such as alveolar rhabdomyosarcoma cell lines (*6*).

Translin, a 228-amino acid single-strand binding protein, contains two distinct domains: a putative transmembrane helix, which may facilitate interactions between translin and microtubule proteins (*6*), and a leucine zipper domain in the carboxy terminus (*2*, *3*). There is compelling evidence that the leucine zipper plays an important role in protein−protein interactions of translin; these may be critical for its DNA-binding activity (*3*, *7*, *8*). Studies with the yeast two-hybrid system demonstrated that the leucine zipper is essential for multimerization (*7*). While a translin octamer is detected by electron microscopy when translin binds to single-stranded DNA (*3*), dimeric translin has also been reported (based on studies with nonreducing SDS−PAGE, glycerol concentration gradient, and gel shift assays) (*7*). It was also reported that the dimer is stabilized by disulfide bond formation involving Cys-225 (*7*).

Our recent sedimentation velocity and equilibrium studies indicated that translin exists as an oblate ellipsoid octamer without reversible monomeric or dimeric species detectable under the experimental conditions. Translin octamer was found to bind single-stranded DNA with a 1:1 stoichiometry (*9*).

This paper will present evidence for several conclusions. The two site-directed mutants, C58S and C225S, demonstrate the following: First, the two -SH groups in translin are distinguishable by their reactivity. Second, only the pyrene maleimide-labeled Cys-225 residues displayed excimer formation, indicating that Cys-225 residues are located in close proximity; hence, subunits associate in a tail-to-tail configuration. Third, time-resolved spectral measurements reveal that the pyrene excimer formation is both prompt and complete. Fourth, time-resolved anisotropy reveals only local motion and the tumbling of a complete octamer. Fifth, disulfide bonds do not play an obligatory role in subunit interactions. These studies shed new light on the association of translin, laying a foundation for studies of the protein−DNA complex.

EXPERIMENTAL PROCEDURES

Plasmid Construction. The plasmid was constructed as described previously (*9*). The clone encoding human translin cDNA (IMAGE Consortium (LLNL) clone ID 668197) was obtained from Research Genetics (Huntsville, AL). The coding sequence of translin was amplified by PCR using the primers TR1−5′-GAGGGATCCTCTGTG AGCGAGATC TTCGTG-3′ and TR2−5′-GAGGTCGACCTATTTTTCAA-CACAAG CTGC-3′. These primers were designed to contain single *Bam* HI and *Sal* I sites (underlined), respectively. The initial ATG encoding Met was omitted to prevent internal initiation when translin is expressed as a recombinant fusion protein. The PCR reaction was performed in the presence

*To whom correspondence should be addressed.
Georgetown University Medical Center.
‡ National Institutes of Health.

10.1021/bi015901e CCC: $22.00
Published on Web 02/14/2002

of *Taq* polymerase, and the purified PCR product was directionally cloned into the *Bam* HI/*Sal* I site of the pQE9 vector (Qiagen) resulting in pQE9-translin. The correct sequence of the protein was confirmed by automated sequencing on an ABI prism instrument (Vincent T. Lombardi Cancer Center Core Facility, Washington, DC).

Site-Directed Mutagenesis. Mutants C58S and C225S were constructed through site-directed mutagenesis using the QuikChange kit (Stratagene) with the following primers:

5C58S: 5′-GGACATTCCAAAGAGGAGTTTGAAAGC-TCG

3C58S: 5′-CGAGCTTTCAAACTCCTCTTTGGAATGT-CC

5C225S: 5′-GGAGACGGCAGCAGCTAGTGTTGAAAAAT-AG

3C225S: 5′-CTATTTTTCAACACTAGCTGCTGCCGT-CTCC

(the sites of the mutated bases are underlined). The correct sequences of the mutants were confirmed by automated sequencing on an ABI prism instrument (Vincent T. Lombardi Cancer Center Core Facility).

Protein Expression and Purification. The protein expression and purification were performed as described previously (*9*). pQE-translin was transformed into BL21(DE3)[pREP4] *Escherichia coli*. A freshly saturated 5-mL overnight culture was used to innoculate 500 mL of LB medium in the presence of 100 μg/mL ampicillin and 25 μg/mL kanamycin and grown at 37 °C to an absorbance of 0.8 at 600 nm. The culture was then induced with 0.4 mM IPTG,[1] and growth was continued for 3 h at 37 °C. The cells were harvested at 4 °C and resuspended in buffer A (50 mM sodium phosphate, pH 8.0, 1 M NaCl) supplemented with 10 mM imidazole and 5% glycerol. All subsequent purification steps were performed at 4 °C. Lysozyme (0.2 mg/mL) was added to the resuspended cells, and the suspension was incubated on ice for 1 h. Subsequently, 10 mM β-mercaptoethanol and 1 mM PMSF were added to the suspension, and the sample was sonicated on ice with a Fisher dismembrator model 300 in alternating cycles until the lysate was no longer viscous. The lysate was centrifuged at 10000*g* for 30 min to remove the cellular debris. One milliliter of 50% Ni-NTA slurry (QIAGEN) per 4 mL of lysate was added to the supernatant solution, and it was incubated for 1 h on a rotary shaker on ice. This lysate−resin mixture was then loaded into an empty column, and the resin was washed with a 20× resin volume of buffer A supplemented with 80 mM imidazole. The protein was eluted with 250 mM imidazole in buffer A. The eluted samples were then dialyzed against 50 mM sodium phosphate, pH 7.4, 100 mM NaCl, 1 mM DTT, 1 mM EDTA, and 5% sucrose. Protein concentrations were assayed by the Bradford method, using BSA as a standard (*10*).

DTNB Reactions. Prior to the DTNB reactions, the protein samples were dialyzed overnight against 1.5 L of buffer B containing 50 mM Tris-HCl, pH 8, 100 mM NaCl, and 1 mM EDTA at 4 °C. After dialysis, the protein samples were spun for 30 min at 10 000 rpm at 4 °C to remove any precipitates using a TOMY MdTX-150 micro refrigerated centrifuge. Kinetic experiments were initiated by the addition of DTNB to 1 mL of protein samples at 23 °C, and changes in absorbance at 412 nm were recorded using the HP 8452A UV−Vis spectrophotometer.

Pyrene Maleimide Labeling. Protein samples were first dialyzed overnight and centrifuged, identically to the DTNB reactions. Two microliters of saturated pyrene maleimide in acetone was then added to the supernatant solutions of the protein samples and mixed. This procedure was repeated every five minutes for a total of 30 min or seven additions. The samples were then dialyzed overnight in 1.5 L of buffer B at 4 °C. The concentration of pyrene maleimide on the protein was determined using an extinction coefficient for pyrene maleimide of 40 000 cm^{-1} M^{-1} at 340 nm (*11*).

Steady-State and Time-Resolved Fluorescence Measurements. Steady-state fluorescence measurements were performed using a Fluorolog-3 spectrofluorometer with 10-mm Glan-Thompson polarizers operated under magic angle conditions. Samples were excited at 338 nm in a 1-mL H-cuvette (NSG 52H). The emission spectrum was scanned twice, and then averaged with both excitation and emission slits at 5 nm.

Time-resolved fluorescence measurements were performed by the time-correlated single-photon counting technique as described previously (*12*, *13*) with the following modifications: Samples were excited at 335 nm using a synchronously pumped, frequency doubled, cavity dumped dye laser (repetition rate 800 kHz, pulse width 5 ps, average UV power < 200 μW). The channel width was either 46 or 183 ps, and the data were collected in 512 channels. Fluorescence decay surfaces were collected under magic angle conditions by stepping the emission monochromator in increments of 10 nm in the range of 350−550 nm. Assuming that fluorescence decay follows a multiexponential law, the total intensity may be calculated as:

$$I(t, \lambda) = \sum_{i}^{n} \alpha_i(\lambda) e^{-t/\tau_i}$$

The 20 decays were simultaneously analyzed according to the global procedure (*14*) with the relative amplitudes α_i and the decay constants τ_i the numerical parameters recovered. Fluorescence intensities at each wavelength were expressed as $\alpha_i\tau_i$ products, and the relative contribution to the total emission was calculated as $\alpha_i\tau_i/\sum\alpha_i\tau_i$ (*15*). The anisotropy decay was analyzed with a sum of discrete exponential functions such that:

$$r(t) = \sum_{j}^{m} \beta_j e^{-t/\phi_j}$$

To generate the anisotropy decay $r(t)$, the fluorescence at 400 nm (the monomer region) was monitored through a film polarizer oriented parallel or perpendicular to the vertical excitation polarization and alternatively recorded. The parameters of the anisotropy decay β_j and ϕ_j were recovered by the "sum and difference" method assuming the nonassociative model (*16*). For each sample, 10 pairs of intensity decays were measured sequentially and summed to calculate the anisotropy decay. The G factor was reduced to unity with

[1] Abbreviations: DTNB, 5,5′-dithiobis(2-nitrobenzoic acid); DTT, dithiothreitol; EDTA, ethylenediaminotetraacetate; EST, expressed sequence tag; His-translin, hexa-histidine-tagged translin; IPTG, isopropyl-β-D-thiogalactoside; NTA, nitrilotriacetate; PCR, polymerase chain reaction; PM, pyrene maleimide; PMSF, phenylmethylsulfonyl fluoride; DAS, decay associated spectra.

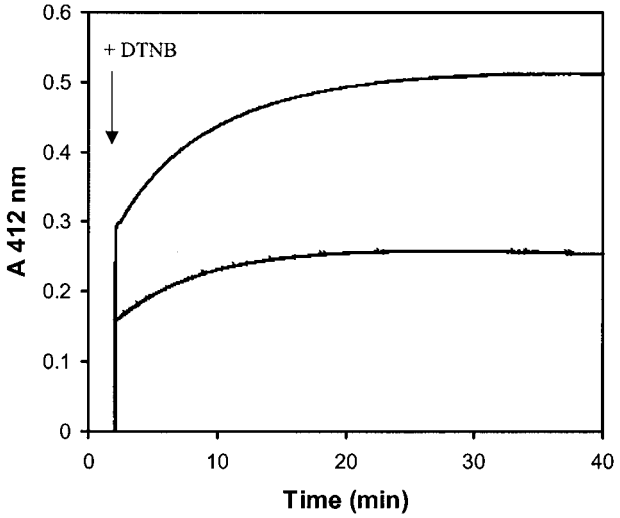

FIGURE 1: Kinetics of DTNB reactions with translin. The reaction was initiated by the addition of 40 μL of 5 mM DTNB to 1 mL each of 17.9 μM (top curve) and 8.9 μM (bottom curve) translin in buffer B at 23 °C, and the kinetic data were measured at 412 nm. The measurements were repeated twice, and the average data were plotted. Deviations between the two measurements were approximately within the line thickness (± 2%).

a wedge depolarizer placed 1 cm from the entrance slit of the monochromator. For both experiments, the best fit between the theoretical curve and the data was evaluated from a plot of weighted residuals, the autocorrelation function of the weighted residuals, and the χ^2 value.

RESULTS

DTNB Reaction with Translin. Translin contains Cys-58 and Cys-225 residues. The number of reactive -SH groups of translin was estimated by reaction with DTNB using the procedure of Ellman (*17*). DTNB reacts with sulfhydryl groups via a disulfide exchange reaction. The TNB anions released as a result of the DTNB reaction represent the quantity of reactive sulfhydryl groups. The concentration of TNB anion was determined spectrophotometrically using an extinction coefficient of 13 600 cm^{-1} M^{-1} at 412 nm (*17*).

Prior to the DTNB reaction, the protein sample was dialyzed against buffer B containing 50 mM Tris, pH 8.0, 100 mM NaCl, and 1 mM EDTA at 4 °C to remove DTT. Kinetic studies were performed by the addition of 40 μL of 5 mM DTNB to 1 mL of 17.9 μM translin in buffer B at 23 °C. As illustrated in Figure 1, the formation of TNB proceeds rapidly at first, followed by a more gradual increase characteristic of a biphasic reaction. The absorbance at 412 nm eventually reached 0.496, which corresponds to a TNB concentration of 36.5 μM. The experiment was repeated using half the concentration of translin (9 μM). Again, the reaction was biphasic, with a rapid change followed by a gradual increase in the formation of TNB. The absorbance at 412 nm eventually reached 0.242, which corresponds to a TNB concentration of 17.8 μM. These results indicate that the molar ratios of reacted -SH to translin monomer were 2.04 and 1.99 for the samples with two different concentrations, in agreement with the number of cysteine residues deduced from the DNA sequence.

DTNB Reactions with Translin C58S and C225S Mutants. The observed kinetic data led to the hypothesis that one -SH group reacts rapidly, while the other reacts slowly. To test this hypothesis, two site-directed mutant proteins, C58S and C225S, were constructed and purified. Kinetic experiments with DTNB were performed by the addition of 20 μL of 5 mM DTNB to 1 mL each of 15.4 μM C58S and 15.6 μM C225S in buffer B at 23 °C. As shown in Figure 2, the reaction proceeds virtually instantaneously with C58S, while C225S reacts much more slowly. The absorbance at 412 nm reached a plateau at 0.202 (15.3 μM) for C58S and 0.216 (15.9 μM) for C225S. The molar ratios of the number of -SH per translin monomer were 0.99 for C58S and 1.02 for C225S. The experiment was repeated by halving the concentration of both protein samples, yielding similar stoichiometries, as shown in Figure 2. From these data, Cys-58 and Cys-225 residues can be clearly designated as the slow and fast reacting -SH groups, respectively.

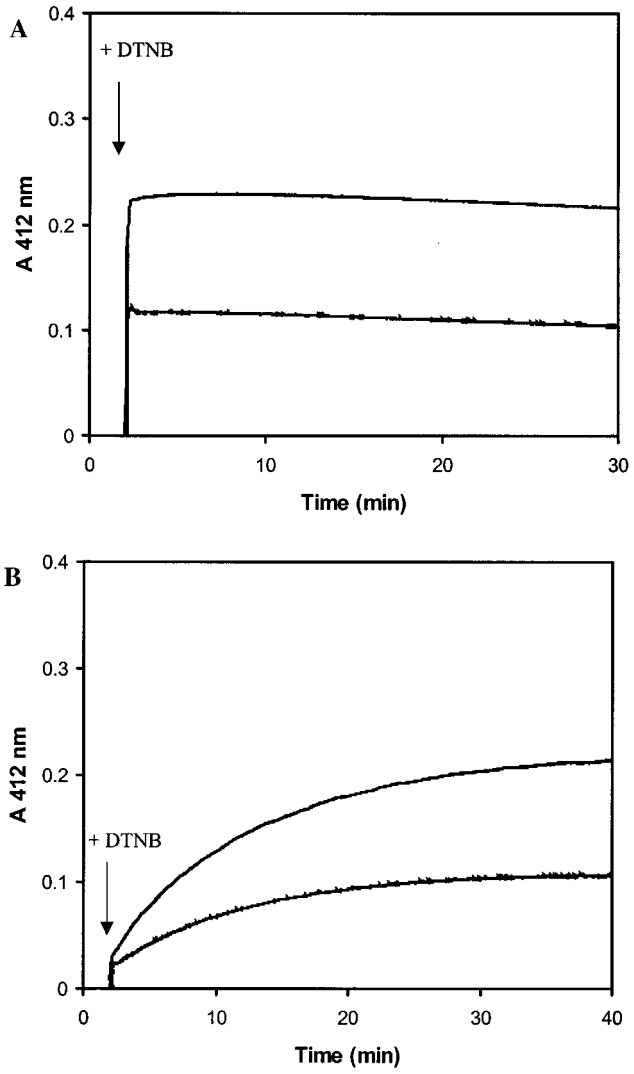

FIGURE 2: Kinetics of DTNB reactions with translin C58S and C225S mutants. DTNB reactions (A) with 7.7 μM (bottom curve) and 15.4 μM (top curve) of translin C58S mutant and (B) with 7.8 μM (bottom curve) and 15.6 μM (top curve) of translin C225S mutant. The reactions were initiated by the addition of 40 μL of 5 mM DTNB to 1 mL each of translin mutants in buffer B at 23 °C, and the kinetic data were measured at 412 nm. The measurements were repeated twice, and the average data were plotted. Deviations between the two measurements were approximately within the line thickness (± 2%).

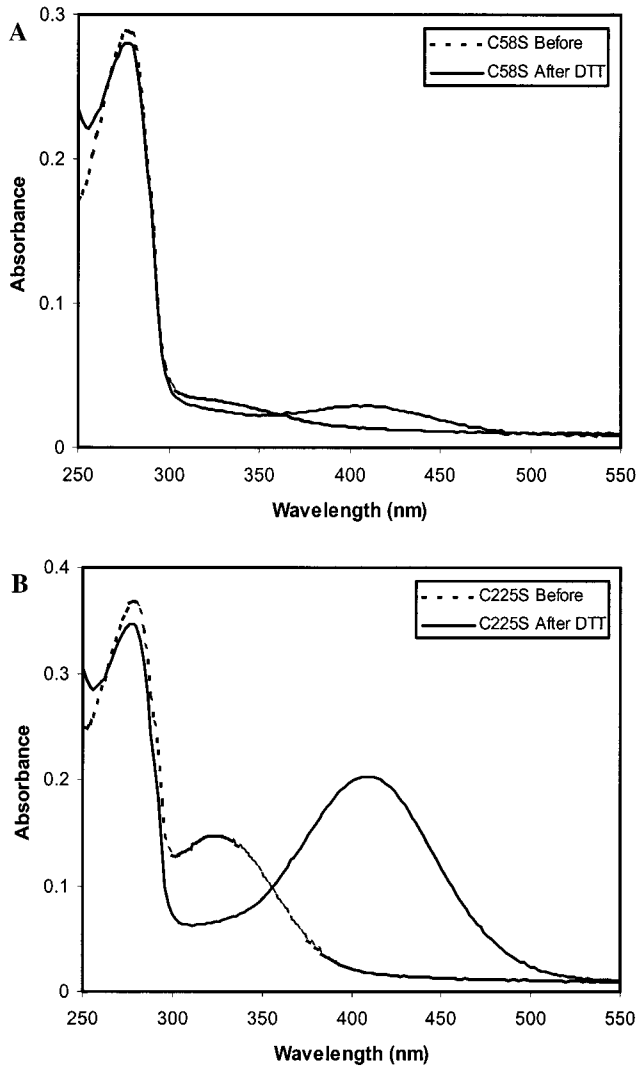

FIGURE 3: Absorption spectra of DTNB-modified translin mutants. Absorption spectra of dialyzed DTNB-reacted (A) 11 μM C58S and (B) 13.1 μM C225S mutants from the kinetic studies shown in Figure 2. Dashed and solid lines represent before and after the addition of 2.0 μL of 100 mM DTT.

When two cysteine residues are located in proximity, these cysteines can sometimes form a DTNB-induced disulfide bond. In a DTNB reaction, one of the TNB groups attaches to the protein and the other becomes a free TNB anion. Subsequently, the proximal sulfhydryl group can attack the mixed disulfide bond between the TNB group and the protein, forming a new disulfide bond between two sulfhydryl groups and releasing that TNB group as a free anion. Thus, the quantitation of TNB groups remaining bound to the protein can determine the absence or presence of DTNB-induced disulfide bond formation. To test this possibility for translin, the DTNB-modified proteins were dialyzed against buffer B to remove any free TNB anions. After dialysis, the absorption spectra of the two mutant samples were recorded. DTT was then added to cleave TNB groups from the protein (to release TNB anions). As illustrated in Figure 3A, only a small fraction of TNB remains bound to the C58S mutant and is detected in the absorbance at 324 nm. The addition of DTT produced ~0.1 mol of TNB anion per mole of the protein, as indicated by absorbance at 412 nm. This accounts for only 10% of the total TNB anion released, as shown in Figure 2A, indicating that pairs of Cys-225 residues easily form a DTNB-induced disulfide bond. On the other hand, 1.04 mol of bound TNB anions per mol of the protein was observed for the DTNB-modified C225S mutant (Figure 3B), which closely agrees with the value shown in Figure 2B. Taken together, these results suggest that Cys-58 residues are not proximate, because no significant level of DTNB-induced disulfide bond formation was detected.

Steady-State Fluorescence Studies with Pyrene Maleimide-Labeled Translin Mutants. After determining that both cysteine residues are reactive, site-specific fluorescent labeling of these mutants was performed under native conditions. Use of an extrinsic fluorescence probe offers many advantages, since desired fluorescent properties of the probe can be selected to characterize subunit interactions and elucidate local structural information. Pyrene maleimide (PM), a -SH specific probe, was selected for its long decay times and specifically for its ability to generate excimer formation.

Initially, each of the two translin mutants was labeled with PM in buffer B at 4 °C. The labeling ratios were 0.79 for C58S and 0.89 for C225S, as determined by the extinction coefficient of PM. The maximum absorption peak was 345 nm for both samples, slightly red-shifted when compared to the 340 nm of free pyrene (data not shown). In addition, the emission spectra of both samples were also altered: the sharp emission peaks (at 375 and 395 nm) of free dye were not displayed by these samples (Figure 4). These changes are because *S*-[*N*-(1-pyrene) succinimido] cysteine, a product of the reaction of the sulfhydryl group of a cysteine residue with the olefinic double bond of the maleimide moiety of *N*-(1-pyrene) maleimide, undergoes a pH-dependent slow cleavage of the succinimido ring by either aminolysis or hydrolysis (*11*, *18*−*21*).

Pyrene maleimide labeling was subsequently performed at pH 7.2 to minimize the ring opening process. The labeling ratios were 0.92 for C58S mutant and 0.84 for C225S mutant. As shown in Figure 5, emission spectra of samples labeled at pH 7.2 show two sharp emission peaks that were not observed with samples labeled at pH 8. Thus, the ring-opening process was significantly reduced at pH 7.2.

Further, there is an additional spectral change in the emission of two PM-labeled samples. Emission spectra of the PM-225 mutant (PM attached to C58S mutant) prepared at both pH 7.2 and 8 exhibit a red-shifted emission feature that peaks around 480 nm; this was not observed in spectra of the PM-58 mutant (PM attached to C225S mutant) (Figures 4 and 5). This emission band is indicative of an "excimer" (excited-state dimer). The excimer forms by stacking interactions between an excited monomer and a ground-state monomer. This has been used as a diagnostic tool in examining proximity between attachment sites (*11*, *22*−*27*).

The emission peak around 480 nm disappeared when PM-225 mutant was denatured with 6 M guanidine-HCl, confirming that pyrene excimer formation is dependent on intact intersubunit interactions. Intermolecular excimer fluorescence was not observed with the PM-58 mutant. Thus, only pyrenes attached to Cys-225 residues are close enough to form an excimer. Given the C-terminal location of the C225 residue, these results suggest that translin subunits interact in a tail-to-tail configuration to form an octamer.

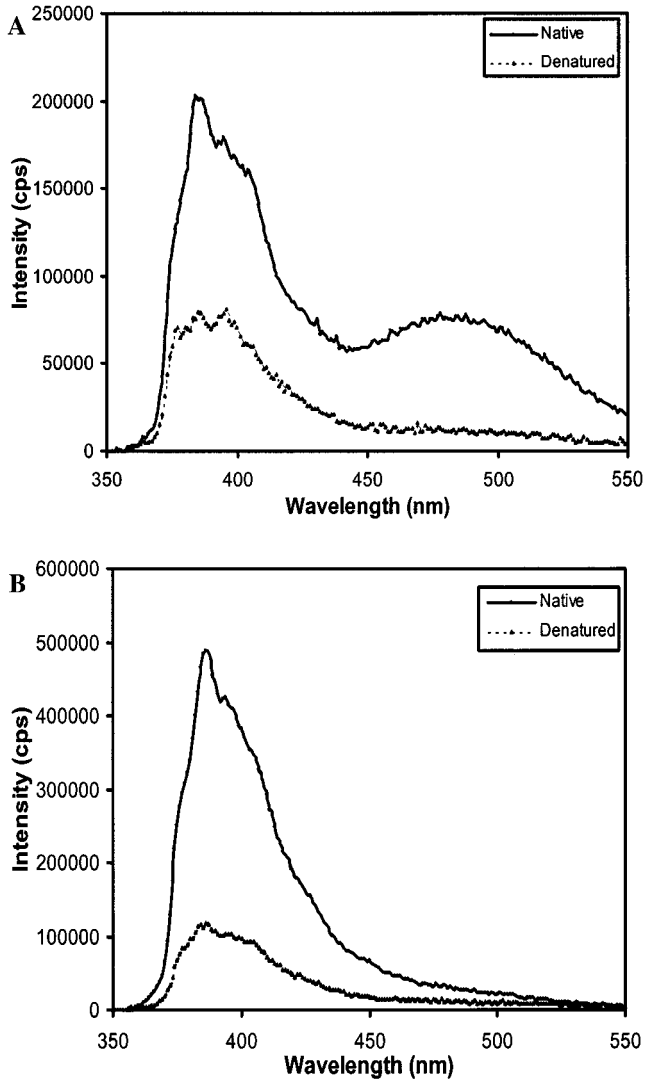

FIGURE 4: Emission spectra of pyrene maleimide labeled translin C58S and C225S mutants. (A) Fluorescence emission spectra of 65.2 nM PM-225 mutant in buffer B at 23 °C (solid line) and in 6 M guanidium HCl at 23 °C (triangles with dashed line). (B) Fluorescence emission spectra of 62.8 nM PM-58 in buffer B at 23 °C (solid line) and in 6 M guanidium HCl at 23 °C (triangles with dashed line). Emission spectra were scanned with an excitation wavelength of 338 nm with 5 nm band paths in both excitation and emission.

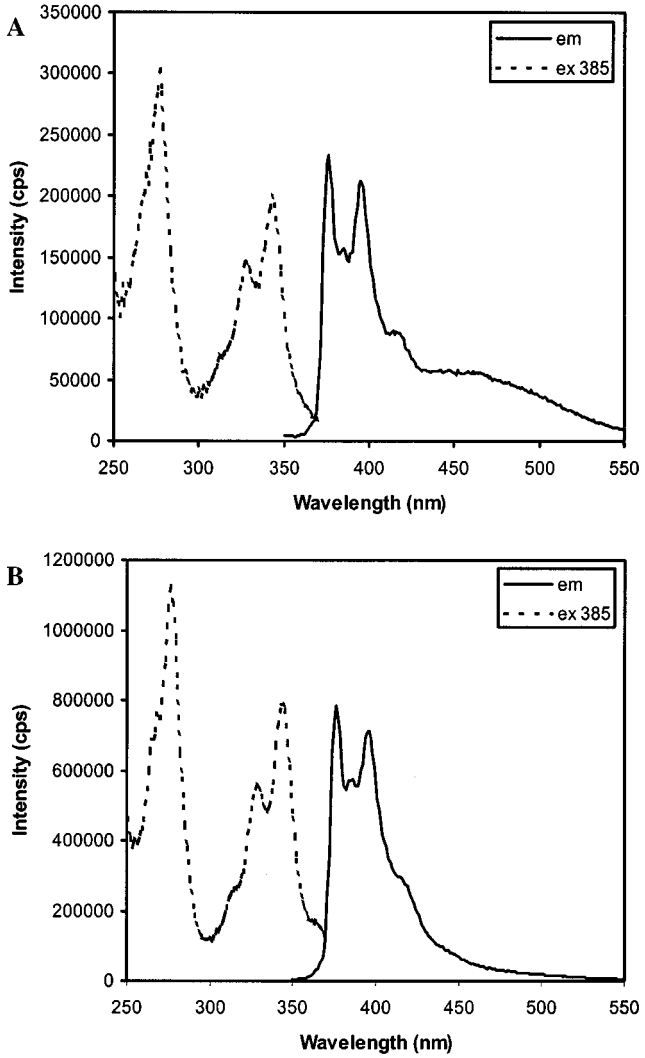

FIGURE 5: Excitation and emission spectra of pyrene maleimide labeled translin mutants. Translin mutants were labeled with pyrene maleimide in PBS buffer, pH 7.2, with 1 mM EDTA. The excitation and emission spectra were plotted with (A) PM-225 mutant and with (B) PM-58 mutant. The excitation spectra were scanned with an emission wavelength of 385 nm, and the emission spectra were scanned with an excitation wavelength of 340 nm with 5 nm band paths in both excitation and emission under magic angle conditions.

Time-Resolved Fluorescence Studies with Pyrene Maleimide- Labeled Translin Mutants. Time-resolved measurements were performed to both quantify the excimer formation process by DAS and to discern the size of the translin complex by emission anisotropy decays. For DAS, decay curves were collected under magic angle conditions in increments of 10 nm in the range of 350−550 nm at 23 °C. The anisotropy decays were collected at 400 nm through a film polarizer oriented parallel or perpendicular to the vertical excitation polarization. The 20 magic angle decay curves were simultaneously analyzed according to a global fitting procedure to generate DAS (*14*), and the anisotropy decay was analyzed with a sum of discrete exponential functions (*15*).

Decay-Associated Spectra (DAS). The decay surface was best fit by analysis with three decay components for both PM-225 and PM-58 mutants, labeled at pH 7.2. The recovered lifetimes were 2.03, 9.43, and 40.15 ns for the PM-225 mutant and 1.58, 8.53, and 46.31 ns for the PM-58 mutant. Preexponential factors, α_i, and intensities, $\alpha_i\tau_i$, corresponding to each of the lifetimes are plotted as a function of wavelength (DAS, Figures 6 and 7). As can be seen in Figure 6, the pyrene excimer fluorescence (peak at 480 nm) was observed only for the PM-225 mutant.

The formation of excimers can often be modeled using simple two-state excited-state reaction kinetics, as explained in Birks (*23*) and Laws et al. (*28*). The complexities of excimer formation in a membrane environment were explored in Davenport et al. (*29*), using schemes for interpreting DAS described in Davenport et al. (*30*) for proton transfer. Basically, the acquisition of DAS in a heterogeneous system allows one to assess the contributions of fast and slow formation kinetics. Fortunately, the excimer process is effectively "irreversible", i.e., the excimer does not form excited-state monomer upon dissociation, only ground states. This simplification leads to DAS that contain only three possible model configurations: X > Y, Y > X and unreacted

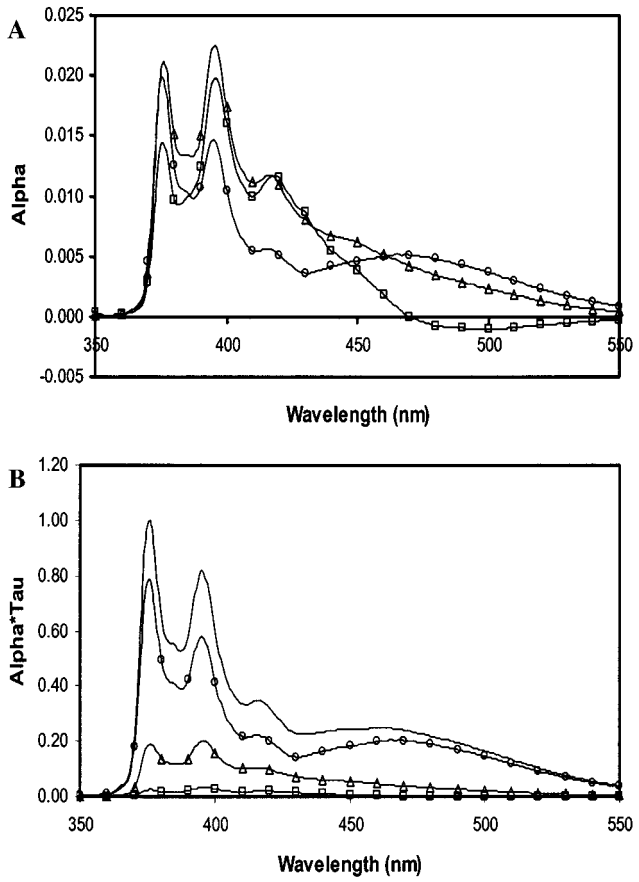

FIGURE 6: Decay-associated spectra of the PM-225 mutant. Decay curves were collected with 8.2 μM PM-225 mutant at 10 nm intervals and two different channel widths (46 and 183 ps). All of the decay curves were simultaneously analyzed, and the results were normalized to the steady-state spectrum. Three decay times were recovered from the global analysis and preexponential factor, α_i (A) and intensity, $I_i = \alpha_i\tau_i$ (B) are shown normalized to unity. □ α_i and I_i for $\tau_i = 1.7$ ns, △ α_i and I_i for $\tau_i = 9.0$ ns, ○ α_i and I_i for $\tau_i = 39.6$ ns, − Steady-state spectrum.

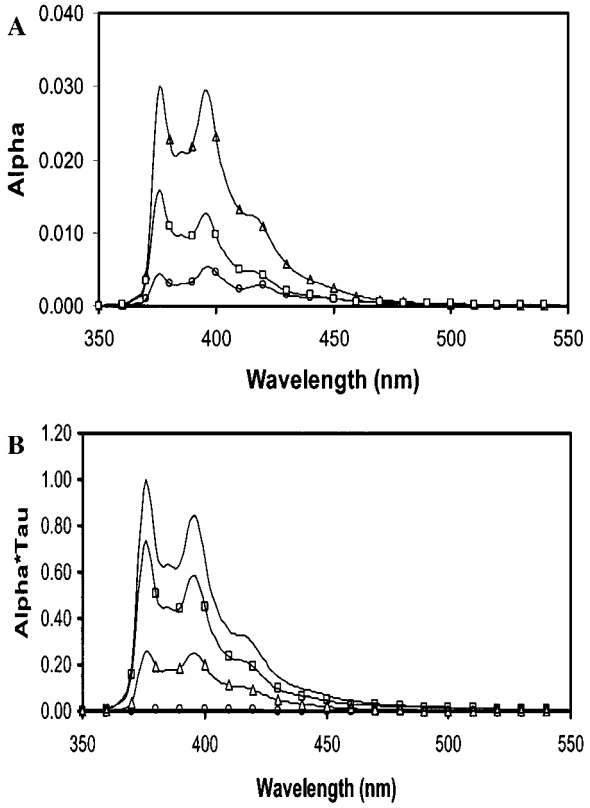

FIGURE 7: Decay-associated spectra of the PM-58 mutant. Decay curves were collected with 3.3 μM PM-58 mutant at 10-nm intervals and analyzed as in Figure 7. Three decay times were recovered from the global analysis and preexponential factor, α_i (A) and intensity, $I_i = \alpha_i\tau_i$ (B) are shown normalized to unity. ○ α_i and I_i for $\tau_i = 1.6$ ns, △ α_i and I_i for $\tau_i = 8.5$ ns, □ α_i and I_i for $\tau_i = 46.3$ ns, − Steady-state spectrum.

monomer. X is the sum of rates depopulating that group of monomers, Y the excimers. If we denote the species DAS, or SAS (*31*) of the monomer as A(λ) and the excimer B(λ), the X > Y case yields a pair of DAS with [A(λ) − B(λ)] associated with $\tau = 1/X$ and [B(λ)] with $\tau = 1/Y$. When X < Y, the DAS [A(λ) + B(λ)] goes with $\tau = 1/X$ and [−B(λ)] with $\tau = 1/Y$. In this way, the short lifetime is always associated with the negative-going DAS (the rise time in the excimer region). In heterogeneous cases, it is not always straightforward to split the observations into these basic categories; the classification process can be complicated by accidental degeneracy (X from one set of pyrenes nearly matches Y from another group) and by prompt formation (the formation of excimers within the lower time resolution of the instrument).

Degeneracy can only be inferred, unless one can somehow adjust the mixture of populations in each group, while prompt formation can be detected by summing amplitude DAS and searching for any excimeric emission (this relies on the fact that the sum of all such DAS leads to the apparent "time zero" spectrum).

As shown in the DAS of the PM-225 mutant (Figure 6), clear evidence of excimer formation is present in the region above 470 nm, where a negative DAS corresponds to a rise time of 1.7 ns. If we had captured all of the excimer formation in this rising term, this X > Y case would have yielded a positive excimer-only spectrum DAS [B(λ)] that mirrors the negative-going DAS about the *x* axis for all wavelengths where monomer is absent (>470 nm or so). As mentioned above, the apparent zero-time spectrum should contain only the monomer spectrum [A(λ)], *unless* we fail to resolve very fast formation. This sum of amplitudes has an excimer shoulder; clearly, we miss some prompt formation. Given the impulse response function of our instrument (FWHM <100 ps), these prompt excimers must form in the first 50 ps. The detailed compartmental analysis of the DAS would require additional knowledge of the system, such as a manipulation that alters the "prompt" vs ns populations of excimers. This is beyond the scope of the current study.

At present, the DAS of the PM-225 mutant allows us to conclude that (i) Virtually all excited pyrenes yield excimer, as no isolated monomeric DAS is evident (unless masked by degeneracy). (ii) The excimer formation is rapid. (iii) In fact, some excimers are in contact immediately upon excitation. The combination of linker group spacings and the known geometry of pyrene stacking yields a maximum -SH to -SH distance between C225S in adjacent subunits at 20 Å (*24*).

Time-Resolved Emission Anisotropy. Time-resolved emission anisotropy is an effective tool for the assessment of molecular size, shape, and flexibility (*32*−*35*). The molecular weight (in thousands) of rigid, nearly spherical globular

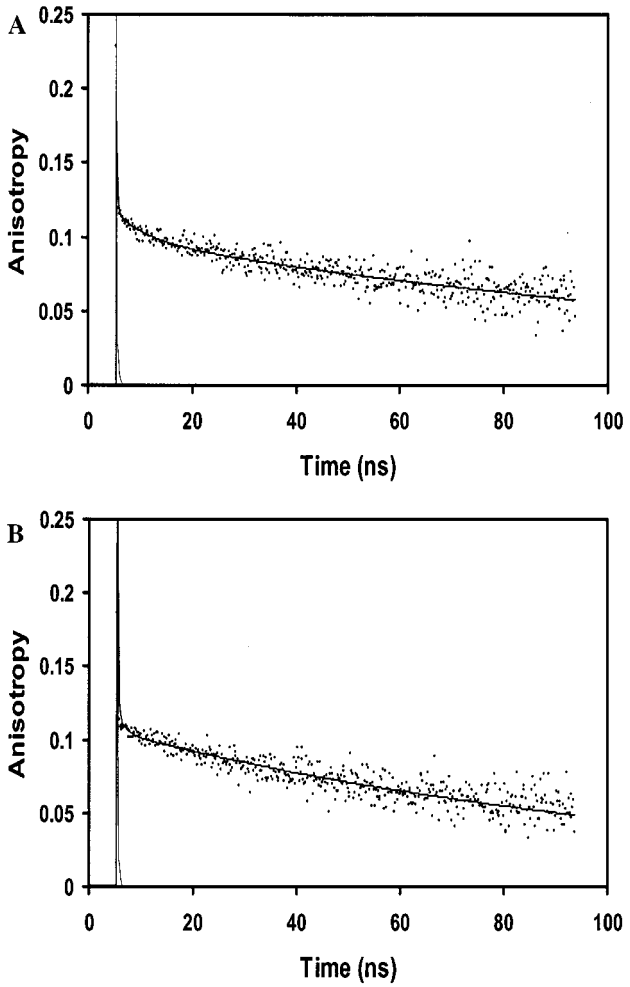

FIGURE 8: Time-resolved emission anisotropy of the PM-225 and PM-58 mutants. Anisotropy decays with (A) 8.2 μM PM-225 mutant and (B) 3.3 μM PM-58 mutant. Anisotropy values were calculated using the "sum and difference" model. For each mutant, the lamp profile, (−) and experimental data points (.) are shown, along with the result of a properly convolved fitting function. The recovered parameters were for PM-225 $\beta_1 = 0.1$ $\phi_1 = 144$ ns [90% confidence between 122 and 181 ns], and $\beta_2 = 0.04$, $\phi_2 = 1.7$ ns. For PM-58, $\beta_1 = 0.104$ $\phi_1 = 115$ ns [90% confidence between 96 and 135 ns], and $\beta_2 = 0.01$ $\phi_2 = 1.5$ ns. Both analyses could be refined somewhat by the addition of a third component <150 ps, which may reflect either ultrafast local motion or a small amount of scattered light.

proteins with moderate hydration at room temperature is *approximately* twice the rotational correlation time (Φ) in ns (more detailed comparisons can be made with refined estimates of hydration level, shape, etc). Nonspherical (esp. very prolate) proteins will have at least biexponential decay rotational correlation times, (Φ), due to the disparity between long and short axis friction. In such cases, the two or more ϕ all exceed that of a sphere with the same volume. The presence of segmental mobility (either of the probe or of a local portion of the protein) also yields at least biexponential anisotropy decay, with a short ϕ appropriate for the volume of the small segment. The ratio of preexponentials yields an estimate of the angular range (e.g., "cone angle") for such local motions.

The time-resolved emission anisotropy decays of pyrene maleimide-labeled translin mutants are shown in Figure 8. Both mutants provide qualitatively the same data: limited but rapid (<2 ns) motions reduce the anisotropy to ~0.103, followed by a slow (>100 ns) rotational diffusion of the overall molecule. The differences between the long ϕ (115 ns for the PM-58 mutant, 144 ns for the PM-225 mutant) are only marginally significant; this is in accord with the expected oblate shape [even if the two transition dipoles were exactly along short and long axes, the correlation time ratio would be much less than the axial ratio (*33*)]. The absence of a term with a correlation time appropriate for dimer (~30 ns) is in accord with our prior analytical ultracentrifugation studies (*9*). Most important, the long correlation time matches our expectations for an octameric species in both cases.

DISCUSSION

Translin contains two cysteine residues, Cys-58 and Cys-225. Previous studies had suggested that Cys-225 forms a disulfide bond that stabilizes the dimeric form of translin (*7*). Our recent sedimentation studies, however, showed that the protein exists as an octamer in solution without detectable monomeric or dimeric species (*9*). In the present work, we have specifically characterized the role of these cysteine residues in intersubunit interactions of translin octamer.

Addressing this problem, we first studied the kinetics of the DTNB reaction with translin. As depicted in Figure 1, the reaction rate was biphasic. There was an initial (almost instantaneous) reaction upon mixing translin and DTNB. This was followed by a slower reaction. The molar ratio of modified -SH groups to protein was 2:1, as quantified by the ratio of TNB anion formed to monomeric protein. These data suggest that Cys-225 and Cys-58 residues react with DTNB at different rates, although other sources of biphasic behavior (such as colligative heterogeneity) could not be excluded. Further DTNB reactions employing two site-directed mutants provided clear evidence that the "instantaneous" reaction was signatory of the C58S mutant, while the slow reaction was observed with the C225S mutant. It is likely that Cys-225, being near the C-terminus of translin, is relatively exposed to the solvent and free to react with DTNB, while Cys-58 is either sterically or environmentally hindered.

It is known that the DTNB reaction can induce the formation of disulfide bonds when two sulfhydryl groups reside very near each other (*36*−*38*). A free sulfhydryl group can displace sulfhydryl-bound TNB to release TNB anion and form a new disulfide bond. We were able to observe this DTNB-induced disulfide formation in the C58S mutant, but not in the C225S mutant. This was evidenced by the observation of TNB anion release only from the DTNB-modified C225S mutant upon addition of DTT (Figure 3B). Because the samples were dialyzed to remove any free TNB anions in solution from the original DTNB reaction, the only TNB anions seen after adding DTT must be from TNB bound to the protein. Hence, there was little TNB bound to the DTNB-reacted C58S mutant. The TNB groups initially conjugated to the protein were presumably released upon formation of intersubunit disulfide bonds. We conclude that these Cys-225 residues are proximate allowing formation of a DTNB-induced disulfide bond.

An additional way to examine the proximity of Cys-225 residues is detection of pyrene excimer fluorescence. Thus, pyrene maleimide-labeled translin mutants, PM-58 and PM-225, were prepared to localize the observation of pyrene

excimers. To prepare homogeneously labeled mutants, however, one must be aware of the potential complications caused by ring opening (*18*−*21*). In fact, Figures 4 and 5 show such a pH-dependent spectral shift associated with the succinimido ring opening. While the proteins labeled at pH 7.2 show typical pyrene emission, the mutants labeled at pH 8.0 display altered emission spectra. Thus, it is preferable to avoid the complications of PM labeling at alkaline pH, and our conclusions are based on labeling at pH 7.2.

Figures 4 and 5 exhibit an additional spectral feature that is not pH-dependent. The emission spectrum for the PM-225 mutant shows an emission band above 470 nm characteristic of a pyrene excimer (Figures 4A and 5A). Upon denaturing the PM-225 mutant to dissociate the subunits, we observed the disappearance of this red-shifted emission. This intermolecular excimer fluorescence was *not* observed from the PM-58 mutant (Figures 4B and 5B).

Pyrene excimers arise from complex formation between an excited monomer and a ground-state monomer. Observation of excimer emission depends on two criteria: proximity and orientation. The excited-state monomer must be within a few Å to stack with the ground-state monomer. Further, the excited monomer and ground-state monomer must orient themselves correctly ("twisted stack") after excitation; otherwise, the fluorescence will be quenched. For this reason, while the lack of excimer fluorescence does not exclude the possibility of pyrene−pyrene contact, the observation of excimer fluorescence clearly indicates the proximity between attachment sites (*11*, *22*−*27*). Therefore, our results indicate that only Cys-225 residues from neighboring subunits are close to each other in the octamer.

The time-resolved emission spectra and resultant DAS further elucidate the excimer formation process: the DAS pattern reveals a mix of 2 ns and ultrafast (<50 ps) excimer formation rates, both suggestive of immediate proximity rather than large scale flexibility. The DAS bear no evidence of unreactive excited pyrene monomers, suggesting all labeled Cys-225 sites are eligible for excimer pairing. (Note that the laser power used is minimal and the probability to simultaneously excite more than one pyrene per protein is negligible).

The time-resolved emission anisotropy traces reveal a mix of two depolarization processes: overall tumbling of the octameric ring and a rapid local ("segmental") motion that usually involves only the linker groups and a few residues near the cysteine. Fortunately, the local motion is limited, and the long-lived pyrene yields a wide temporal observation window, so a precise estimate of the global motion is possible. The long correlation times are in accord with expectations for an oblate octameric ring. Moreover, the anisotropy decays yield no sign of dimeric or monomeric species, in accord with our analytical ultracentrifugation studies (*9*).

The data presented in this paper suggested that Cys-225 residues are close enough to each other to form a DTNB-induced disulfide bond and to rapidly form excimers. Wu et al. (*7*) previously suggested that disulfide bonds stabilize dimer formation. Our data, however, support neither the spontaneous formation of disulfide bonds nor the formation of dimer. Our protein samples differ in that Wu et al. used a GST fusion protein, while we employed a his-tag motif. We believe that these N-terminal modifications are unlikely to alter oligomerization dominated by the C-terminal leucine zipper. Disulfide bonds do not appear to play an obligatory role in the formation and stability of the octamer: free cysteines in translin were available to and occupied by pyrene maleimide, yet it was still capable of forming the proper oligomeric species.

It is, therefore, apparent that translin does not require disulfide bonds to form an octamer, suggesting the leucine zipper domain plays the predominant quaternary role in the formation of octomer. The leucine zipper motif has previously been shown to be important for dimerization and DNA binding of many nucleic acid binding proteins (*39*). For example, a number of transcription regulatory proteins such as CREB, Jun, and myc require dimerization of the leucine zipper domain to bind DNA. Interestingly, Zuccola et al. (*40*) described a similar annular structure consisting of eight subunits for the RNA-binding hepatitis delta antigen; it also contains a leucine zipper motif. Apparently, this type of structure is present in a variety of nucleic-acid binding proteins, and it could be envisioned that this form plays an important role in binding and "protecting" the end of the free single-stranded nucleic acids. Future studies with site-directed mutations of the leucine zipper will help us further probe the function of translin.

REFERENCES

1. Rabbitts, T. H. (1994) *Nature 372*, 143−149.
2. Wu, X. Q., Gu, W., Meng, X. H., and Hecht, N. B. (1997) *Proc. Natl. Acad. Sci. U.S.A. 94*, 5640−5645.
3. Aoki, K., Suzuki, K., Sugano, T., Yasaka, T., Nakaharam K., Kuge, O., Omori, A., and Kasai, M. (1995) *Nat. Genet. 10*, 167−174.
4. Aoki, K., Inazawa, J., Takahashi, T., Nakahara, K., and Kasai, M. (1997) *Genomics 43*, 237−241.
5. Kasai, M., Matsuzaki, T., Katayanagy, K., Omori, A., Maziarz, R. T., Strominger, J. L., Aoki, K., and Suzuki, K. (1997) *J. Biol. Chem. 272*, 11402−11407.
6. Chalk, J. K., Barr, F. G., and Mitchell, C. D. (1997) *Oncogene 15*, 1199−1205.
7. Wu, X. Q., Xu, L., and Hecht, N. B. (1998) *Nucleic Acids Res. 26*, 1675−1680.
8. Hohjon, H., and Singer, M. F. (1996) *EMBO J. 15*, 630−639.
9. Lee, P. S., Fuior, E., Lewis, M. S., and Han, M. K. (2001) *Biochemistry 40*, 14081−14088.
10. Bradford, M. M. (1976) *Anal. Biochem. 72*, 248−254.
11. Han, M. K., Knutson, J. R., Roseman, S., and Brand, L. (1990) *J. Biol. Chem. 265*, 1996−2003.
12. Lee, S. P., Censullo, M. L., Kim, H. G., Knutson, J. R., and Han, M. K. (1995) *Anal. Biochem. 227*, 295-.
13. Lee, S. P., Xiao, J., Knutson, J. R., Lewis, M. S., and Han, M. K. (1997) *Biochemistry. 36*, 173−1180.
14. Knutson, J. R., Beechem, J. R., and Brand, L. (1983) *Chem. Phys. Lett. 102*, 501−507.
15. Knutson, J. R., Walbridge, D. G., and Brand, L. (1982) *Biochemistry 21*, 4671−4679.
16. Beechem, J. M., Gratton, E., Ameloot, M., Knutson, J. R., and Brand, L. (1991) in *Topics in Fluorescence Spectroscopy* (Lakowicz, J. R., Ed.) Vol. 2, pp 241−305, Plenum Press, New York.
17. Ellman, G. L. (1959) *Arch. Biochem. Biophys. 82*, 70−77.
18. Gregory, J. D. (1955) *J. Am. Chem. Soc. 77*, 3922−3933.
19. Smyth, D. G., and Tuppy, H. (1968) *Biochim. Biophys. Acta 168*, 173−180).
20. Heitz, J. R., Anderson, C. D., and Anderson, B. M. (1968) *Arch. Biochem. Biophys. 127*, 627−636.
21. Wu, C. W., Yarbrough, L. R., and Wu, Y. H. (1976) *Biochemistry 15*, 2863−2868.

22. Förster, T. (1969) *Angew. Chem., Int. Ed. 8*, 333.
23. Birks, J. B. (1970) *Photophysics of Aromatic Molecules*, Wiley-Interscience, London.
24. Lehrer, S. S., and Fasman, G. D. (1965) *J. Am. Chem. Soc. 87*, 4678.
25. Betcher-Lange, S., and Lehrer, S. S. (1978) *J. Biol. Chem. 253*, 3757.
26. Zama, M., Bryan, P. M., Harrington, R. E., Olins, A. L., and Olins, D. E. (1978) *Cold Spring Harbor Symp. Quantum Biol. 42*, 31.
27. Lehrer, S. S. (1995) *Subcellular Biochemistry* (Biaswas, B. B., and Roy, S., Eds.) Vol. 24, pp 115−139, Plenum, New York.
28. Laws, W. R., and Brand, L. *J. Phys. Chem*. (1979) *83*, 795−802.
29. Davenport, L., Knutson, J. R., and Brand, L. (1989) in *Subcellular Biochemistry 14*, pp 145−148, Plenum, New York.
30. Davenport, L., Knutson, J. R., and Brand, L. (1986) *Biochemistry 25*, 1186−1195.
31. Beechem, J. M., Ameloot, M., and Brand, L. *Chem. Phys. Lett. 120*, 466−472.
32. Wahl, Ph. (1980) in *Time-Resolved Fluorescence Spectroscopy in Biochemistry and Biology* (Cundall, R. B., and Dale, R. E., Eds.*)* Plenum, New York.
33. Beechem, J. M., Knutson, J. R., and Brand, L. (1986) *Biochem. Soc. Trans. 14*, 832.
34. Shen, F., Triezenberg S. J., Hensley, P., Porter, D., and Knutson, J. R. (1996) *J. Biol. Chem 271*, 4819−4837.
35. Tcherkasskaya, O., Ptitsyn, O. B., and Knutson, J. R. (2000) *Biochemistry 39*, 1879−1889.
36. Boross, L. (1969) *Arch. Biochem. Biophys. 2*, 47−51.
37. Stoops, J. K., and Wakil, S. (1981) *J. Biol. Chem. 256*, 5128−5133.
38. Digani, Y., and Digani, C. (1979) *Biochemistry 18*, 5917−5923.
39. Busch, S. J., and Sassone-Corsi, P. (1990) *Trends Genet. 6*, 36−40.
40. Zuccola, H. J., Rozelle, J. E., Lemon, S. M., Erickson, B. W., and Hogle, J. M. (1998) *Structure 6*, 821−830.

BI015901E